Computers, Materials & Continua CMC, vol.65, no.3, pp.2351-2363, 2020

New SAR Imaging Algorithm via the Optimal Time-Frequency Transform Domain

Zhenli Wang[1, *], Qun Wang[1], Jiayin Liu[1], Zheng Liang[1] and Jingsong Xu[2]

Abstract: To address the low-resolution imaging problem in relation to traditional Range Doppler (RD) algorithm, this paper intends to propose a new algorithm based on Fractional Fourier Transform (FrFT), which proves highly advantageous in the acquisition of high-resolution Synthetic Aperture Radar (SAR) images. The expression of the optimal order of SAR range signals using FrFT is deduced in detail, and the corresponding expression of the azimuth signal is also given. Theoretical analysis shows that, the optimal order in range (azimuth) direction, which turns out to be very unique, depends on the known imaging parameters of SAR, therefore the engineering practicability of FrFT-RD algorithm can be greatly improved without the need of order iteration. The FrFT-RD algorithm is established after an analysis of the optimal time-frequency transform. Experimental results demonstrate that, compared with traditional RD algorithm, the main-lobe width of the peak-point target of FrFT-RD algorithm is narrow in both range and azimuth directions. While the peak amplitude of the first side-lobe is reduced significantly, those of other side-lobes also drop in various degrees. In this way, the imaging resolution of range and azimuth can be increased considerably.

Keywords: Fourier transform, fractional Fourier transform, synthetic aperture radar, range doppler algorithm.

1 Introduction

Synthetic aperture radar (SAR) is a form of radar that is used to create two-dimensional images or three-dimensional reconstructions of objects [Zhang, Liang and Yang (2018)], such as landscapes. The most common imaging algorithms consist of Range Doppler (RD), Chirp Scaling (CS), ωK and SPECAN. RD algorithm is a classical method for SAR imaging processing thanks to its easy operability and high computational efficiency [Smith (1991)]. However, its strength is greatly compromised by its weakness: the quality of the acquired images is low, hence greatly reduces the applicability of the algorithm. The Secondary Range Compression (SRC), a modified algorithm, is able to improve the

[1] Department of Computer Information and Network Security, Jiangsu Police Institute, Nanjing, China.

[2] Research Fellow Faculty of Engineering and Information Technology, University of Technology Sydney, New South Wales, Australia.

[*] Corresponding Author: Zhenli Wang. Email: dongwen3619@sina.com.

Received: 05 June 2020; Accepted: 24 July 2020.

imaging accuracy of SAR, but its dependence on the azimuth frequency [Cumming and Wong (2005)] becomes yet another problem that is difficult to resolve. The application of FrFT to SAR imaging processing has been a focus of research in recent years [Ramona, Nicolas, Grégoire et al. (2016); El-Mashed, Zahran, Dessouky et al. (2013); Wang and Jiang (2018); Huang, Xia, Gao et al. (2019); Zhang and Jiang (2016); Wang and Wang (2020)], and researchers are particularly interested in the fractional orders.

Two-dimensional peak spectrum search [Fouts and Pace (2002)] in fractional Fourier domain is proposed to determine the optimal transform order of FrFT for Linear Frequency Modulation (LFM) parameter estimation. This method has very good stability, but a tremendous amount of calculation is required, and the precision of parameter estimation is reduced due to the limited amount of data samples. By using geometric transformation relationship, the optimal order of FrFT for LFM signals [Capus and Brown (2003)] can be obtained, but the corresponding FrFT cannot replace the Fourier Transform (FT) in traditional RD algorithm to achieve signal reconstruction. The literature [Amein and Soraghan (2007)] has applied FrFT to traditional CS algorithm, and obtained a higher signal-to-noise ratio (SNR) and a better focused image in airborne SAR system. The literature [Chen, Zhao, Chen et al. (2014)] has measured the frequency modulation of SAR echo signals by way of local optimal processing and has calculated the optimal order of FrFT. This algorithm is effective in improving the imaging performance of missile-borne SAR according to its experimental results, but it is not universally applicable. In an attempt to address the low resolution problem of traditional RD algorithm, this paper begins with the use of FrFT analysis to obtain the optimal processing order of SAR raw signals, then establishes a new SAR imaging algorithm to complete pulse compression and range migration in the corresponding FrFT domain, and finally concludes with a presentation of experimental results and an analysis of the measured data of the space-borne RADARSAT-1.

2 SAR imaging model

A three dimensional Cartesian coordinate system XYZ is chosen as the reference system, the height of SAR platform is h meters over the horizon, and the velocity is v m/s uniform along the X axis. Points $\mathrm{P}(x, y, z)$ and $\mathrm{T}(x_{\mathrm{T}}, y_{\mathrm{T}}, z_{\mathrm{T}})$ are the position vectors of the SAR platform and the target respectively, where point T is located at the center of SAR imaging swath. From the spatial geometric relationship shown in Fig. 1, the slant distance R_0 between T and P is as follows

$$R_0 = \sqrt{(x - x_T)^2 + (y - y_T)^2 + (z - z_T)^2} \tag{1}$$

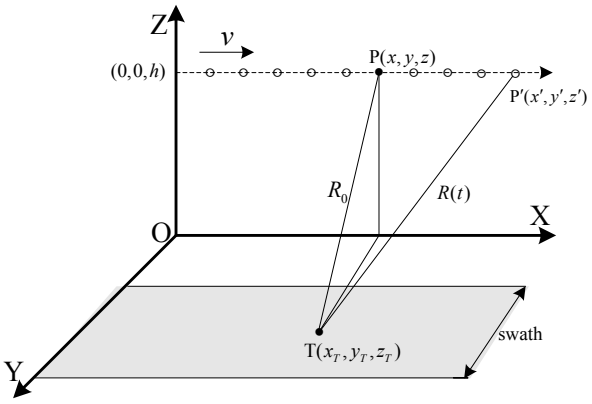

Figure 1: Spatial geometric illustration of SAR imaging

It is assumed that the slant distance between P′ and T is $R(t)$, and t is a slow time variable when the SAR platform moves to any position on the flight path. The LFM signals emitted by SAR at any position P′ is shown in Eq. (2).

$$s_r(\tau) = \text{rect}\left(\frac{\tau}{T_P}\right)\exp\left(\text{j}2\pi f_c\tau + \text{j}\pi\kappa_r\tau^2\right) \tag{2}$$

where τ is the fast time variable, T_P is the pulse width, f_c is the carrier frequency, κ_r is the modulation frequency of SAR echo signals, c is the light speed and $\text{rect}(\cdot)$ is the rectangular window function. The pure echo signal reflected by target T is shown in Eq. (3).

$$s(\tau,t) = \left\{\text{rect}\left[\frac{\tau-\frac{2R(t)}{c}}{T_P}\right]\exp\left[\text{j}\pi\kappa_r\left[\tau-\frac{2R(t)}{c}\right]^2+\text{j}2\pi f_c\tau\right]\right\}\times\left\{W_a(t)\exp\left[-\text{j}\frac{4\pi}{\lambda}R(t)\right]\right\} \tag{3}$$

where λ is the wavelength, $W_a(t)$ is the azimuth window function, which is related to the shape of antenna beam as well as the filter weighting. To simplify the calculation, $W_a(t)$ is taken as rectangular window $W_a(t) = \text{rect}(t/T_a)$, where T_a is the synthetic aperture time.

3 Order analysis of SAR echo signals using fractional Fourier transform

The fractional Fourier transform of the continuous-time signal $f(x)$ is defined as

$$F_\alpha[f](u) = \int_{-\infty}^{\infty} K_\alpha(u,x)f(x)dx \tag{4}$$

where $K_\alpha(u,x)$ is the kernel function of FrFT as shown in Eq. (5), α is the rotation angle and $\alpha = -\mu\times\pi/2$, μ is the order of FrFT.

$$K_\alpha(u,x) = A_\alpha\cdot\exp\left\{j\pi\left[\left(x^2+u^2\right)\cot\alpha - 2ux\csc\alpha\right]\right\} \tag{5}$$

where $A_\alpha = \sqrt{1-\mathrm{j}\cot\alpha}$, and $\alpha \neq n\pi$. If $\alpha = 2n\pi$, $K_\alpha(u,x) = \delta(u-x)$, and if $\alpha = (2n+1)\pi$, $K_\alpha(u,x) = \delta(u+x)$. Considering the time delay, Eq. (4) is substituted for the SAR range signals in Eq. (2).

$$F_\alpha[S_r](u) = \int K_\alpha(u,\tau)\,\mathrm{rect}\left[\frac{\tau - \dfrac{2R(t)}{c}}{T_P}\right] \times \exp\left[\mathrm{j}2\pi f_c\left(\tau - \frac{2R(t)}{c}\right) + \mathrm{j}\pi\kappa_r\left(\tau - \frac{2R(t)}{c}\right)^2\right] d\tau \tag{6}$$

To simplify the calculation, the following settings are substituted into Eq. (6) without producing adverse effect on the optimal order analysis of FrFT, where $f_c = 0$, $R(t) = 0$, and $W_r(\tau) = \mathrm{rect}(\tau/T_P)$.

$$\begin{aligned} F_\alpha[S_r](u) &= \int_{-\infty}^{\infty} K_\alpha(u,\tau) W_r(\tau) \exp\left(\mathrm{j}\pi\kappa_r\tau^2\right) d\tau \\ &= \int_{-\infty}^{\infty} \sqrt{1-\mathrm{j}\cot\alpha} \cdot \exp\left\{\mathrm{j}\pi\left[\left(\tau^2+u^2\right)\cot\alpha - 2u\tau\csc\alpha\right]\right\} \times W_r(\tau)\exp\left(\mathrm{j}\pi\kappa_r\tau^2\right) d\tau \\ &= A_\alpha \exp\left(\mathrm{j}\pi u^2\cot\alpha\right) \int_{-\infty}^{\infty} \exp\left[\mathrm{j}\pi\left(\tau^2\cot\alpha - 2u\tau\csc\alpha\right)\right] \times W_r(\tau)\exp\left(\mathrm{j}\pi\kappa_r\tau^2\right) d\tau \end{aligned} \tag{7}$$

where $A_\alpha = \sqrt{1-\mathrm{j}\cot\alpha}$. The inequality $|\tau| \le \Delta t/2$ is substituted into Eq. (7), where Δt is the time width of the range signal samples and $\Delta t > T_p$.

$$F_\alpha[S_r](u) = A_\alpha \exp\left(\mathrm{j}\pi u^2\cot\alpha\right) \int_{-\Delta t/2}^{\Delta t/2} \exp\left[\mathrm{j}\pi\left(\tau^2\cot\alpha - 2u\tau\csc\alpha\right)\right] \times \exp\left(\mathrm{j}\pi\kappa_r\tau^2\right) d\tau \tag{8}$$

The Eq. (8) can be calculated by fast discrete algorithm of FrFT. Since the actual SAR raw signals are usually time-limited and band-limited, which satisfies the tight support conditions on the time and frequency axes, dimensional normalization [Zhao, Deng and Tao (2005)] can be used in the analysis of FrFT. However, these two references consider only time interval rather than discrete sampling and fail to give the expression of the optimal order of FrFT. In this paper, a defined coordinate system (υ,η) is used to replace the original time-frequency coordinate system (τ, f), where $\upsilon = \tau/\gamma$, $\eta = f\gamma$, and $\gamma = \sqrt{\Delta t/\Delta f}$ is the scale factor with time dimension. It is assumed that the sampling length and frequency of SAR range signals is N_r and F_r, respectively. When the dimensional normalization is used to the SAR range signals, the modulation frequency and the rotation angle become κ_r' and α' respectively. So the SAR range signals in the coordinate system (υ,η) is limited to a discrete sampling interval $\left[-\sqrt{N_r}/2, \sqrt{N_r}/2\right]$, where $\sqrt{N_r} = \sqrt{\Delta t \cdot \Delta f}$. The normalized SAR raw signals sampled with $1/\sqrt{N_r}$ are consistent with the original discrete data.

Let $\upsilon \in \left[-\sqrt{N_r}/2, \sqrt{N_r}/2\right]$, κ_r' and α' substitute κ_r and α respectively in Eq. (8).

$$
\begin{aligned}
&F_{\alpha'}[S_r](u)\\
&= A_\alpha \exp\left(\mathrm{j}\pi u^2 \cot\alpha'\right)\int_{-\frac{\sqrt{N_r}}{2}}^{\frac{\sqrt{N_r}}{2}} \exp\left[\mathrm{j}\pi\left(\frac{N_r}{F_r^2}\upsilon^2\cot\alpha' - 2u\upsilon\frac{\sqrt{N_r}}{F_r}\csc\alpha'\right)\right]\times\exp\left(\mathrm{j}\pi\kappa_r'\frac{N_r}{F_r^2}\upsilon^2\right)d\upsilon\frac{\sqrt{N_r}}{F_r}\\
&= \frac{A_\alpha\sqrt{N_r}}{F_r}\exp\left(\mathrm{j}\pi u^2\cot\alpha'\right)\times\int_{-\frac{\sqrt{N_r}}{2}}^{\frac{\sqrt{N_r}}{2}}\exp\left[\mathrm{j}\pi\left(\frac{N_r\cot\alpha'+N_r\kappa_r'}{F_r^2}\upsilon^2 - 2u\frac{\sqrt{N_r}\csc\alpha'}{F_r}\upsilon\right)\right]d\upsilon
\end{aligned}
\tag{9}
$$

Let the variable $y=\frac{\sqrt{2\left(N_r\cot\alpha'+N_r\kappa_r'\right)}}{F_r}\left(\upsilon-\frac{u\sqrt{N_r}F_r\csc\alpha'}{N_r\cot\alpha'+N_r\kappa_r'}\right)$, so $d\upsilon=\frac{F_r}{\sqrt{2\left(N_r\cot\alpha'+N_r\kappa_r'\right)}}dy$,

$y_1=\frac{\sqrt{2\left(N_r\cot\alpha'+N_r\kappa_r'\right)}}{F_r}\times\left(\frac{\sqrt{N_r}}{2}-\frac{u\sqrt{N_r}F_r\csc\alpha'}{N_r\cot\alpha'+N_r\kappa_r'}\right)$, $y_2=\frac{\sqrt{2\left(N_r\cot\alpha'+N_r\kappa_r'\right)}}{F_r}\left(\frac{\sqrt{N_r}}{2}+\frac{u\sqrt{N_r}F_r\csc\alpha'}{N_r\cot\alpha'+N_r\kappa_r'}\right)$.

The above variables are substituted into Eq. (9) as follows.

$$
F_{\alpha'}[S_r](u)=\frac{A_\alpha\sqrt{N_r}}{\sqrt{2\left(N_r\cot\alpha'+N_r\kappa_r'\right)}}\times\exp\left[\mathrm{j}\pi u^2\left(\cot\alpha'-\frac{N_r\csc^2\alpha'}{N_r\cot\alpha'+N_r\kappa_r'}\right)\right]\times\int_{-y_2}^{y_1}\exp\left(\mathrm{j}\frac{\pi}{2}y^2\right)dy \tag{10}
$$

The actual numerical value of modulation frequency κ_r is so great that it may reach up to the level of 10^{12}. Considering the relational equations $\gamma=\sqrt{N_r}/F_r$, $\kappa_r'=\kappa_r/\gamma^2$, the approximate conclusions can be obtained as $y_1\to\infty$, $y_2\to\infty$. So

$$
\begin{aligned}
&\int_{-y_2}^{y_1}\exp\left(\mathrm{j}\frac{\pi}{2}y^2\right)dy=\int_{-\infty}^{\infty}\exp\left(-\mathrm{j}\frac{\pi}{2}y^2\right)dy\\
&=2\left[\int_0^{\infty}\cos\left(-\mathrm{j}\frac{\pi}{2}y^2\right)+\mathrm{j}\sin\left(-\mathrm{j}\frac{\pi}{2}y^2\right)\right]dy
\end{aligned}
\tag{11}
$$

The conclusion $\int_{-y_2}^{y_1}\exp\left(\mathrm{j}\frac{\pi}{2}y^2\right)dy=\sqrt{2}\exp\left(\mathrm{j}\frac{\pi}{4}\right)$ can be obtained based on Eq. (11), which is the two forms of Fresnel integral. It is substituted into Eq. (10) as follows.

$$
F_{\alpha'}[S_r](u)=\frac{A_\alpha\sqrt{2N_r}\exp\left(\mathrm{j}\frac{\pi}{4}\right)}{\sqrt{2\left(N_r\cot\alpha'+N_r\kappa_r'\right)}}\times\exp\left[\mathrm{j}\pi u^2\left(\cot\alpha'-\frac{N_r\csc^2\alpha'}{N_r\cot\alpha'+N_r\kappa_r'}\right)\right] \tag{12}
$$

If the fractional energy spectrum $F_{\alpha'}[s_r](u)$ is highly focused on the axis of the FrFT domain at the rotation angle α', the following equation can be obtained according to Eq. (12), and $F_{\alpha'}[s_r](u)$ becomes an impulse function.

$$
N_r\cot\alpha'+N_r\kappa_r'=0 \tag{13}
$$

Therefore, the optimal order μ_{opt} of the SAR range signals in FrFT domain can be obtained as Eq. (14) by using $\kappa_r'=\kappa_r N_r/F_r^2$, $\alpha'=\frac{\pi}{2}\mu'$, and $\alpha'=\alpha$.

$$
\mu_{\text{opt}}=\mu'=\frac{2}{\pi}\arctan\left(-\frac{F_r^2}{\kappa_r N_r}\right) \tag{14}
$$

where arctan(·) is an arctangent function. For the given SAR echo sampling signals, the modulation frequency κ_r, the sampling length N_r and the sampling frequency F_r in range direction are known, so it is easy to calculate the optimal order μ_{opt} directly according to Eq. (14).

In the expression $K_{\alpha_{\text{opt}}}(u_{\alpha_{\text{opt}}},\tau)=\sqrt{1-\text{j}\cot\alpha_{\text{opt}}}\times\exp\left\{j\pi\left[\left(\tau^2+u_{\alpha_{\text{opt}}}{}^2\right)\cot\alpha_{\text{opt}}-2u_{\alpha_{\text{opt}}}\tau\csc\alpha_{\text{opt}}\right]\right\}$, the coefficient of the fast time variable τ is equal to $-2\pi u_{\alpha_{\text{opt}}}\csc\alpha_{\text{opt}}$, where $\alpha_{\text{opt}}=-\mu_{\text{opt}}\times\pi/2$. In the expression $\exp\left[\text{j}2\pi f_c\left(\tau-\frac{2R(t)}{c}\right)+\text{j}\pi\kappa_r\left(\tau-\frac{2R(t)}{c}\right)^2\right]$, the corresponding coefficient becomes $2\pi f_c-4\pi\frac{\kappa_r R(t)}{c}$. By using the definition of Fourier Transform of impulse function, $\alpha=\alpha_{\text{opt}}$ and $u=u_{\alpha_{\text{opt}}}$, the coefficient of the fast time variable τ in Eq. (6) is assumed to be zero, as can be seen in Eq. (15).

$$-2\pi u_{\alpha_{\text{opt}}}\csc\alpha_{\text{opt}}+2\pi f_c-4\pi\frac{\kappa_r R(t)}{c}=0 \tag{15}$$

According to Eq. (15), the obtained energy spectrum $F_{\alpha'}[S_r](u)$ is highly focused on the axis $u_{\alpha_{\text{opt}}}$ of FrFT domain. The axis $u_{\alpha_{\text{opt}}}$ is shown in Eq. (16).

$$u_{\alpha_{\text{opt}}}=\frac{cf_c-2R(t)\kappa_r}{c\csc\alpha_{\text{opt}}} \tag{16}$$

The SAR echo samples in azimuth direction can be regarded as LFM signals. The analysis of the optimal order in azimuth direction [Wang and Wang (2020)] is similar to range direction, and its expression is given as in Eq. (17) by using FrFT.

$$v_{\text{opt}}=\frac{2}{\pi}\arctan\left(-\frac{F_a^2}{\kappa_a N_a}\right) \tag{17}$$

where κ_a is the modulation frequency, N_a is the sampling length and F_a is the sampling frequency in azimuth direction.

4 Construction of optimal time-frequency transform domain

FrFT, as a generalized Fourier analysis method, can be interpreted as a signal representation method in the FrFT domain, which is obtained by rotating a signal at any angle α counter-clockwise around the origin point in the time-frequency plane. Any fractional order p corresponds to a time-frequency rotation angle α. If it is the optimal order, the energy spectrum of FrFT under the corresponding time-frequency rotation angle is an impulse function as mentioned earlier. Therefore, the optimal order of FrFT and the optimal rotation angle are the unique corresponding relations. When the FrFT is applied to SAR echo signals, the optimal order μ_{opt} in range direction can be calculated according to Eq. (14).

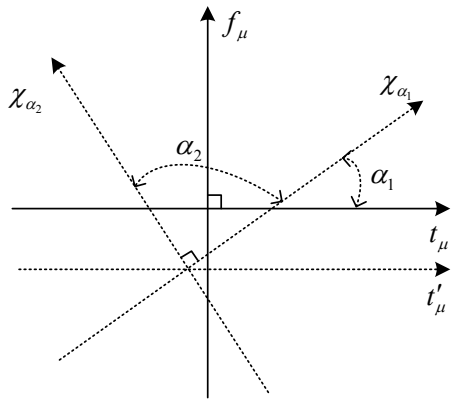

Figure 2: Time-frequency domain rotation illustration of range signals

The corresponding optimal time-frequency rotation angle is $\alpha_1 = -\mu_{\text{opt}} \times \pi/2$, where the negative sign indicates counter-clockwise rotation. Fig. 2 shows the time-frequency rotation illustration of the signals in range direction, where t_μ and f_μ represent the time domain and frequency domain respectively, χ_{α_1} represents the FrFT domain corresponding to FrFT when the rotation angle of the time-domain range signals is α_1, χ_{α_2} represents the FrFT domain when the rotation angle of the signal in the FrFT domain χ_{α_1} is α_2 ($\alpha_2 = \pi/2$), and the order corresponding to α_2 is 1. t'_μ represents the parallel axis of t_μ. It's obvious that $t_\mu \perp f_\mu$, $\chi_{\alpha_1} \perp \chi_{\alpha_2}$. According to the rotation invariance of FrFT, the decomposition form of the range signals in the time-frequency domain (t_μ, f_μ) is equivalent to that in the FrFT $(\chi_{\alpha_1}, \chi_{\alpha_2})$ domain. Assuming that the decomposed signal in χ_{α_1} domain corresponds to the frequency signal in f_μ domain, the decomposed signal in χ_{α_2} domain will also correspond to the time signal in t_μ domain. An analysis of the optimal time-frequency transform of the azimuth signals will come to the same conclusion.

5 Construction of high resolution SAR imaging algorithm

For SAR raw signals, especially the measured data, the rotation angles in time-frequency domain corresponding to the optimal order μ_{opt} in range direction and ν_{opt} in azimuth direction are usually in the first quadrant of time-frequency plane, and the smaller rotation angle will reduce the focusing effect of the signals. By using the results of the previous analysis, the corresponding time-frequency angles can be rotated $\pi/2$, and the optimal orders in the range and azimuth directions should be changed to $1-\mu_{\text{opt}}$ and $1-\nu_{\text{opt}}$ respectively, as can be seen in Fig. 3 for range signals.

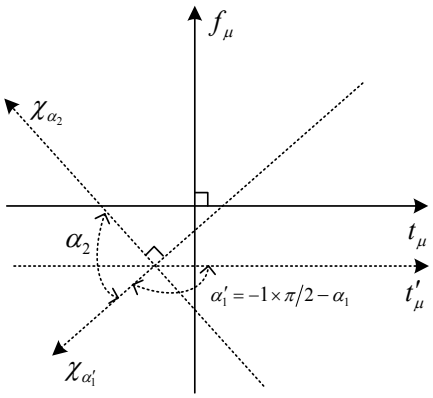

Figure 3: Time-frequency domain rotation illustration of range signals

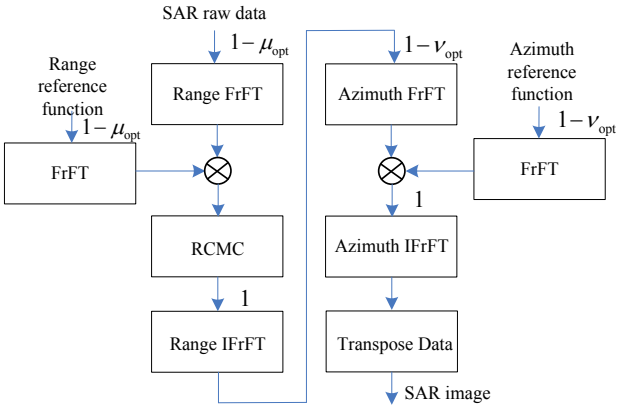

Figure 4: Construction illustrations of FrFT-RD algorithm

Fig. 4 shows the construction illustrations of the proposed SAR imaging algorithm (FrFT-RD). In this algorithm, the original SAR range signals and range compression reference function are both transformed by FrFT with the order to complete range pulse compression and range cell migration correction (RCMC) [Wang and Wang (2020)], and then the range signals are reconstructed by fractional inverse Fourier transform with the order 1. Compared with traditional RD algorithm, the range pulse compression in the proposed algorithm can be better performed because of the optimal time-frequency transform of the range signals, and the corresponding RCMC can be performed with the same operation. The SAR azimuth signals and azimuth compression reference function are both transformed by FrFT with the order to complete azimuth pulse compression based on the range signal processing, and then the azimuth signals are reconstructed by fractional inverse Fourier transform with the order 1. As seen in Fig. 4, the FrFT with the optimal orders in both range and azimuth directions can completely replace the traditional Fourier Transform without increasing the amount of calculation, and the proposed algorithm becomes the traditional RD algorithm when $\mu_{opt} = \nu_{opt} = 0$.

6 Data processing results and analysis

The data processing experiment uses the measured data of Vancouver scene in Canadian RADARSAT-1 fine mode. The traditional RD and FrFT-RD algorithms are used for imaging experiment and analysis. The length of range and azimuth sampling signals are 2464 and 2912, respectively. Figs. 5(a) and 5(b) are the imaging results of the traditional RD and FrFT-RD algorithms, respectively. Figs. 6(a) and 6(b) are the local enlarged SAR images in the yellow rectangular of Figs. 5(a) and 5(b), respectively.

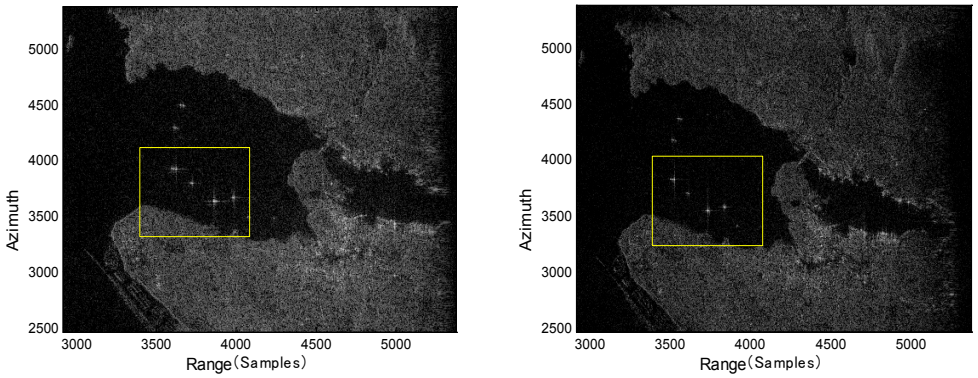

(a) (b)

Figure 5: SAR images of measured data: (a) traditional RD algorithm; (b) FrFT-RD algorithm

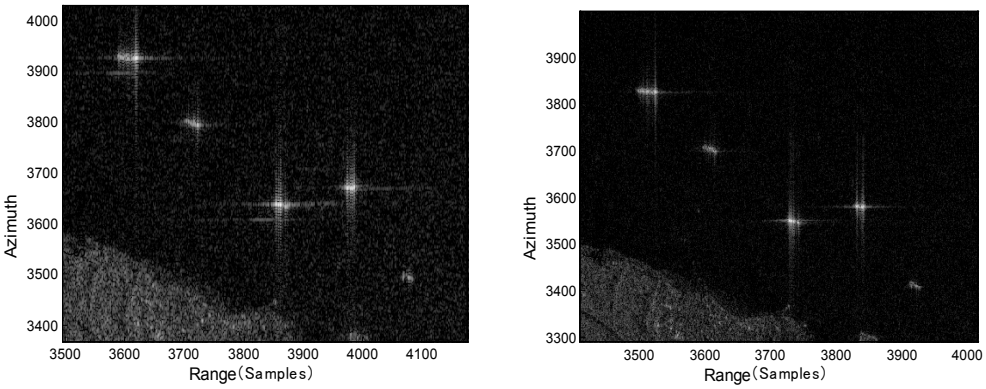

(a) (b)

Figure 6: SAR images of measured data（local magnification）: (a) traditional RD algorithm; (b) FrFT-RD algorithm

By comparing the local magnification images of the two algorithms in Figs. 6(a) and 6(b), it can be seen that the images of the two ship targets obtained by RD algorithm are seriously blurry, the image focusing performance is poor, and the speckle noise on the water surface is obvious. The SAR image obtained by FrFT-RD algorithm can well resolve

the above problems. In this image, the ship target is clear, the speckle noise is small, the water-land boundary is visible, the texture of the land target is distinct, the image contrast is sharp. Therefore, compared with images acquired via RD algorithm, those acquired via FrFT-RD algorithm are more appropriate for target interpretation and recognition. Fig. 7 shows the contours of the interpolated peak-point target by the two algorithms. Fig. 8 shows the profile images of the corresponding target in Fig. 7. The performance comparison of the two algorithms is shown in Tab. 1. As seen in Figs. 7 and 8, the main-lobe width of peak-point target in FrFT-RD algorithm becomes narrower in both range and azimuth directions, the peak amplitude of the first side-lobe decreases significantly, and those of the other side-lobes also decreases in various degrees. According to the experimental data in Tab. 1, the absolute range and azimuth resolution of FrFT-RD algorithm is 3.81 and 12.77 lower than those of RD algorithm, and the corresponding range and azimuth resolution ratios improve 43.39% and 44.02% respectively. The range PSLR (Peak Side Lobe Ratio) and ISLR (Integrated Side Lobe Ratio) of FrFT-RD algorithm are 0.98 dB and 0.36 dB lower than those of RD algorithm respectively. The corresponding results in azimuth direction become 2.59 dB and 2.26 dB respectively.

Table 1: Performance comparison of SAR imaging algorithms

algorithm		resolution /m	PSLR/dB	ISLR/dB
RD	range	8.78	-9.22	-5.41
	azimuth	29.01	-13.53	-11.24
FrFT-RD	range	4.97	-10.20	-5.77
	azimuth	16.24	-16.12	-13.50

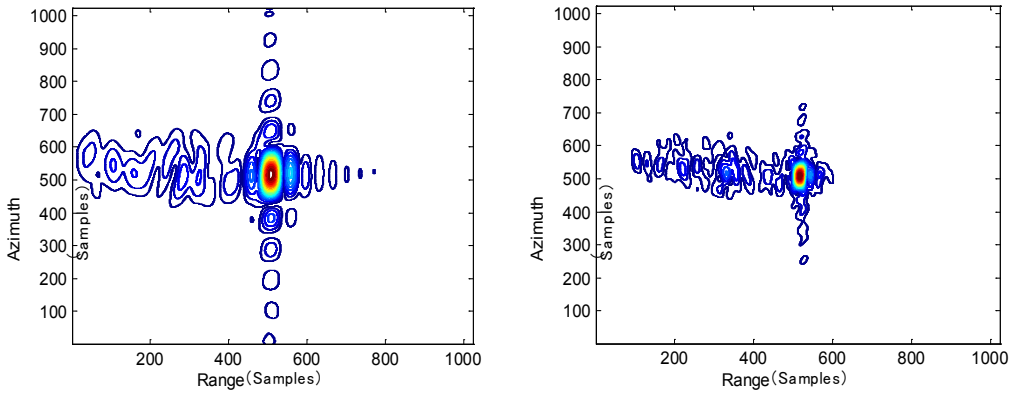

(a) (b)

Figure 7: The contours of the interpolated peak-point target :(a) traditional RD algorithm; (b) FrFT-RD algorithm

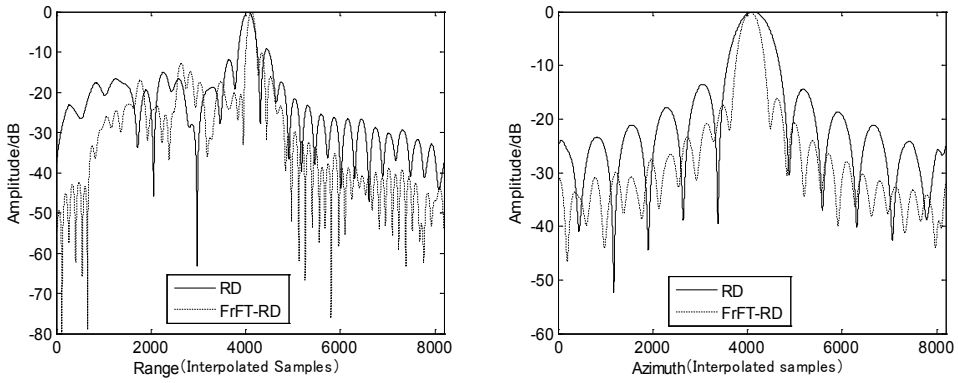

(a) (b)

Figure 8: The profile images of the interpolated peak-point target: (a) the profile images in range direction; (b) The profile images in azimuth direction

7 Discussion

The range resolution of SAR images is generally limited by the bandwidth of the transmitted radar waveform. However, a new algorithm is herein proposed, which is capable of significantly improving the imaging resolution in the range direction. This can be done chiefly because the optimal-order FrFT is adopted to replace traditional Fourier Transform in traditional RD algorithm. The optimal order of FrFT and the optimal rotation angle are the unique corresponding relations. Unlike traditional RD algorithm, the proposed algorithm completes the range pulse compression and RCMC of LFM signals in the specific FrFT domain based on the known imaging parameters of SAR. The FrFT domain of the proposed algorithm has better focusing property for LFM signals. Moreover, now that the azimuth resolution is limited by the Doppler bandwidth as well, high-resolution imaging in the azimuth direction can also be obtained by using specific FrFT domain.

8 Conclusion

A new SAR imaging algorithm is herein presented. It has the advantage of achieving high image resolution by using fractional Fourier Transform instead of Fourier Transform. The proposed algorithm is established based on the unique optimal orders in range and azimuth directions via an analysis of the optimal time-frequency transform of FrFT. The proposed algorithm can be transformed back to traditional RD algorithm when the optimal time-frequency rotation angles of the range and azimuth directions are equal to zero. As far as the measured data of the space-borne RADARSAT-1 are concerned, the assessed results demonstrate that the proposed algorithm performs much better than traditional RD algorithm both in range and azimuth directions. The findings of this work are of practical value in the interpretation of images produced by spaceborne and airborne SAR as well as in target detection and target recognition, thus is widely applicable in the computer visualization.

Funding Statement: This work is supported by the 13th Five-Year Plan for Jiangsu Education Science (D/2020/01/22), JSPIGKZ (JSPI19GKZL405) and Natural Science Research Projects of Colleges and Universities in Jiangsu Province(19KJB510022).

Conflicts of Interest: The authors declare that they have no conflicts of interest to report regarding the present study.

References

Amein, A. S.; Soraghan, J. J. (2007): Fractional chirp scaling algorithm: mathematical model. *IEEE Transactions on Signal Processing*, vol. 55, no. 8, pp. 4162-4172.

Capus, C.; Brown, K. (2003): Short-time fractional Fourier methods for the time-frequency representation of chirp signals. *Journal of the Acoustical Society of America*, vol. 113, no. 6, pp. 3253-3263.

Chen, Y.; Zhao, H. C.; Chen, S.; Zhang, S. N. (2014): An improved focusing algorithm for missile-borne SAR with high squint. *Applied Mechanics and Materials*, vol. 608-609, pp. 761-765.

Cumming, I. G.; Wong, F. H. (2005): *Digital Processing of Synthetic Aperture Radar Data: Algorithms and Implementation*. Artech House, Norwood.

El-Mashed, M. G.; Zahran, O.; Dessouky, M. I.; EI-Kordy, M.; Abd EI-Samie, F. E. (2013): Synthetic aperture radar imaging with fractional fourier transform and channel equalization. *Digital Signal Processing*, vol. 23, no. 1, pp. 151-175.

Fouts, D. J.; Pace, P. E. (2002): A single-chirp false target radar image generator for countering wideband imaging radars. *IEEE Journal of Solid-State Circuits*, vol. 37, no. 6, pp. 751-759.

Huang, P. H.; Xia, X. G.; Gao, Y. S.; Liu, X. Z.; Liao, G. S. et al. (2019): Ground moving target refocusing in SAR imagery based on RFRT-FrFT. *IEEE Transactions on Geoscience and Remote Sensing*, vol. 57, no. 8, pp. 5476- 5492.

Ramona, P.; Nicolas, L.; Grégoire, M.; Guillaume, H.; Rene, G. (2016): Vessel refocusing and velocity estimation on SAR imagery using the fractional fourier transform. *IEEE Transactions on Geoscience and Remote Sensing*, vol. 54, no. 3, pp. 1670-1684.

Smith, A. M. (1991): A new approach to range-Doppler SAR processing. *International Journal of Remote Sensing*, vol. 12, no. 2, pp. 235-251.

Wang, H. Y.; Jiang, Y. C. (2018): Real-time parameter estimation for SAR moving target based on WVD slice and FrFT. *Electronics Letters*, vol. 54, no. 1, pp. 47-49.

Wang, Z. L.; Wang, Q. (2020): On the application of optimal FrFT order for improving the azimuth resolution of range doppler imaging algorithm. *IET Image Processing*, vol. 14, no. 4, pp. 789-793.

Wang, Z. L.; Wang, Q.; Li, F. J.; Wang, S. (2020): High resolution SAR image algorithm with sample length constraints for the range direction. *Computers, Materials & Continua*, vol. 63, no. 3, pp. 1533-1543.

Zhang, D. Y.; Liang, Z. S.; Yang, G. B.; Li, Q. G.; Li, L. D. et al. (2018): A robust forgery detection algorithm for object removal by exemplar-based image inpainting. *Multimedia Tools and Applications*, vol. 77, no. 10, pp. 11823-11842.

Zhang, L.; Jiang, Y. C. (2016): Imaging algorithm of multi-ship motion target based on compressed sensing. *Journal of Systems Engineering and Electronics*, vol. 27, no. 4, pp. 790-796.

Zhao, X. H.; Deng, B.; Tao, R. (2005): Dimensional normalization in the digital computation of the fractional Fourier transform. *Transactions of Beijing Institute of Technology*, vol. 25, no. 4, pp. 360-364.